Intermolecular Coupling in Liquid and Crystalline States of *trans*-*N*-Methylacetamide Investigated by Polarized Raman and FT-IR Spectroscopies

Reinhard Schweitzer-Stenner and Guido Sieler

FB1-Institut für Experimentelle Physik, Universität Bremen, P.O. Box 330440, 28334 Bremen, Germany

Noemi G. Mirkin and Samuel Krimm*

Biophysics Research Division, University of Michigan, Ann Arbor, Michigan 48109

Received: July 24, 1997; In Final Form: October 21, 1997[⊗]

The isotropic and anisotropic Raman spectra of neat *N*-methylacetamide (NMA) at different temperatures between −10 and 60 °C and NMA in acetonitrile were measured in order to spectroscopically compare and characterize the crystallized (T < 28 °C) and liquid states. These plus infrared data were subjected to a self-consistent component band analysis. We found that the amide I band is composed of two subbands in the solid phase and three in the liquid phase. For the former, the subbands at 1633 and 1656 cm^{-1} arise from transition dipole coupling interactions associated with the A_g and B_{2g} species of the crystal unit cell. Depolarization ratio measurements suggest a departure from strict D_{2h} symmetry. The three subbands in the liquid phase reflect different aggregate structures. The lowest frequency band at 1634 cm^{-1} results from an NMA oligomer exhibiting a structure similar to that observed in the ordered crystal phase. The most intense subband shows a significant negative noncoincidence effect, its isotropic component appearing at 1650 cm^{-1} and its anisotropic part at 1655 cm^{-1}. This subband is interpreted as resulting from locally ordered short oligomeric hydrogen-bonded structures. The third subband is at 1675 cm^{-1} and results from isolated non-hydrogen-bonded NMA molecules or from amide I modes of the terminal groups of the above oligomers. Amide III shows a small but detectable positive noncoincidence effect in the liquid phase (2 cm^{-1}), which is also assignable to transition dipole coupling between adjacent molecules in a locally ordered environment. The Raman bands arising from the symmetric bending modes of the two methyl groups are significantly affected by crystallization; the CCH_3 symmetric bending mode becomes depolarized and less intense while the NCH_3 symmetric bending mode gains intensity and becomes polarized. Ab initio calculations of torsional distortions of the CH_3 groups, caused by interactions between adjacent non-hydrogen-bonded NMA molecules in the crystal, qualitatively reproduce these effects.

Introduction

The amide group is a basic repeat unit of biological macromolecules such as peptides and proteins and synthetic polymers such as nylons. The understanding of such polyamide structure and dynamics requires knowledge not only of the intermolecular force field but also of noncovalent coupling between amide groups and between such groups and water molecules of the aqueous environment. These interactions comprise hydrogen bonding, between CO and NH groups of different amides in close proximity and between amide groups and water molecules, and transition dipole coupling mechanisms.[1]

Vibrational spectroscopy is a very sensitive tool for characterizing the above interactions in terms of their types and coupling strengths. This is due to the fact that vibrations of the amide group give rise to several intense bands in the infrared and Raman spectra, termed amide I, II, III, etc., the frequencies and intensities of which depend strongly on the intrinsic electronic properties of the group as well as on amide−side chain and amide−solvent interactions.[1,2]

In this context, numerous investigations have been directed to monosubstituted amides such as formamide ($HCONH_2$)[3] and *N*-methylformamide ($HCONHCH_3$),[4] derivatives such as *N*,*N*-dimethylacetamide ($CH_3CONH(CH_3)_2$),[5] and cyclic amides such as ϵ-caprolactam and 2-azacyclononanone.[5,6] All these molecules have in common that their CO and NH groups have a strong preference for the formation of hydrogen bonds with solvent molecules if this is physically possible. Such hydrogen bonds are strong in aqueous solution and of intermediate strength in organic solvents.[7] Intermolecular hydrogen bonds are also formed between the CO and NH groups of adjacent molecules.[3,8] This can result in hydrogen-bonded chains, which may exist either in a crystalline solid[9] or in the liquid state.

N-Methylacetamide ($CH_3CONHCH_3$, NMA) has been recognized as a useful model system to study hydrogen bonding between peptide groups, such as are found in polypeptides and proteins. Numerous spectroscopic studies have examined its ground- and excited-state structures and dynamics as well as its vibrational spectra.[10] Early X-ray diffraction studies[11a] indicated that NMA has a trans structure in its crystalline phase, with its five heavy atoms coplanar (trans and cis refer to the orientation of CO and NH with respect to the CN bond). Below 10 °C crystallized NMA consists of chains of molecules in which hydrogen bonds between CO and NH groups connect

* Corresponding author. E-mail: skrimm@umich.edu. FAX: 313-764-3323.

[⊗] Abstract published in *Advance ACS Abstracts,* December 15, 1997.

S1089-5639(97)02408-0 CCC: $15.00
Published on Web 01/01/1998

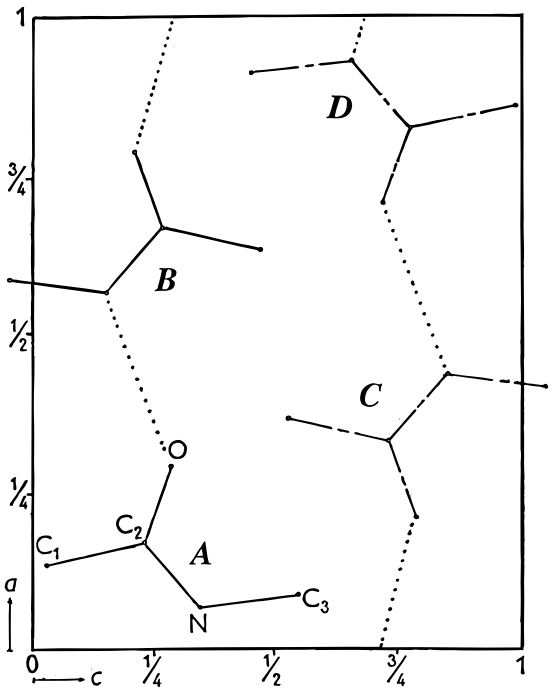

Figure 1. Structure of solid NMA in its ordered (T < 10 °C) phase (from ref 11a).

adjacent molecules in a structure that exhibits D_{2h} symmetry (Figure 1). A small amount of static disorder is present even in this crystalline phase.[11b] A more disordered structure was observed between 10 and 28 °C.[11a] At higher temperatures, neat NMA is in its liquid phase. This is believed to have an even more disordered structure, though one still maintaining some degree of hydrogen bonding.[12]

Vibrational spectroscopic studies on NMA started with the detailed IR investigations by Miyazawa and co-workers.[10a] They observed IR spectra of solid NMA and NMA in organic solvents and provided assignments of the main amide bands. This was followed by polarized IR studies of single-crystal NMA.[10b,c] Ataka et al.[13] measured IR spectra of trans and cis NMA in N_2 matrixes at cryogenic temperatures. Other IR studies on solid NMA with and without an aqueous environment revealed rather complex spectral features, particularly in the high-frequency region between 1000 and 1800 cm^{-1}, which are still not fully understood.[14] Raman spectra of neat NMA have also been reported.[10c,15]

Since these Raman and IR experiments on neat liquid and solid NMA, the availability of more advanced techniques such as FT-IR and UV-Raman has shifted the focus to the spectroscopy of NMA in aqueous or organic solvents.[10d−k] In addition, some UV resonance Raman data on neat liquid NMA were reported by Triggs and Valentini.[5b] They found that the amide I band is composed of two Lorentzian subbands which they assigned to NMA oligomers of various sizes. More recently Chen et al.[10h] measured polarized Raman spectra of neat liquid NMA with visible and UV excitation. Their spectral analysis revealed two Voigtian rather than Lorentzian subbands of amide I at 1646 and 1658 cm^{-1}. While the former appears nearly totally polarized, the latter is completely depolarized. In the IR spectrum amide I appears close to the frequency of the depolarized Raman band. This doublet cannot be explained in terms of different oligomers. It is indicative instead of a noncoincidence effect (NCE), i.e., intermolecular interactions that cause the frequencies of isotropic and anisotropic scattering to separate.[16] The NCE is a well-established phenomenon in the physics of pure liquids and binary mixtures and has been observed for many diatomic molecules,[17] compounds with a carbonyl group,[18] dimethyl sulfoxide,[19] 1,2,5-thiadiazole,[20] chloroform,[21] and monoamides such as formamide and *N*,*N*-dimethylacetamide.[3b]

In many respects NMA is still a relevant system to investigate. It behaves like a highly ordered oligopeptide in the crystal phase while it becomes more disordered in the liquid phase, which makes it more similar to an amorphous polymer. Vibrational spectroscopy is well suited to comparing these phases of NMA with each other and also with NMA dissolved in different types of liquids. In this paper we report polarized Raman spectra of neat NMA measured at different temperatures between −10 and 60 °C with 457 and 384 nm excitation. Thus we obtain spectra of the liquid as well as of the solid state. Moreover we have measured polarized Raman spectra of NMA dissolved in acetonitrile (CH_3CN and CD_3CN). All spectra were subjected to a self-consistent spectral analysis that yielded frequencies, half-widths, and depolarization ratios of all relevant Raman-active bands above 1200 cm^{-1}. The data allow us to describe and compare intermolecular NMA−NMA and NMA−solvent interactions. The Raman band depolarization ratios are utilized to determine the influence of these interactions on the contribution of the $\pi \rightarrow \pi^*$ transition to the Raman cross sections far from resonance.

Material and Methods

Materials. NMA was purchased from Sigma and distilled before use. The concentration of the analyte was 3.0 M for the Raman experiments in CD_3CN and ranged between 0.25 and 1.0 M for measurements of amide I in CH_3CN.

Instrumental Methods. Most of the Raman experiments were carried out using a conventional spectrometer at the University of Michigan. The Raman spectra were measured with 90° scattering geometry. Excitation at 457 nm was obtained from a Coherent argon ion laser. The incident laser beam was polarized perpendicular to the spectrometer's optical axis and focused onto the sample by a $f = 10$ cm lens. Plasma lines of the argon ion laser were eliminated by an optical unit consisting of a mirror, a small grating, and an exit slit of appropriate width. The sample was contained in a thin capillary tube that was situated in a sample holder connected to a thermostat. The scattered light was collected by a lens with 15° angular acceptance and analyzed with a polarizer. A polarization scrambler was placed between the polarizer and the spectrometer entrance slit. The scattered light was dispersed by a Spex Czerny-Turner double monochromator equipped with 2400 grooves/mm holographic gratings. The spectral resolution was 2 cm^{-1}. The light was detected by a photomultiplier.

Another pair of polarized Raman spectra were measured at −10 °C using a Raman spectrometer at the University of Bremen equipped with the 384 nm output of an excimer pumped dye laser. We have used the 488 nm line of the argon ion laser in this laboratory to measure the amide I band of NMA in CH_3CN at different concentrations. Both spectrometers are equipped with CCD cameras, which allow recording of spectra with low intensities. Details of the experimental setup are given elsewhere.[22]

All spectra were subjected to a line shape analysis by the program MULTIFIT.[23] This program allows appropriate baseline corrections, deconvolution of highly overlapped bands by the Fourier self-deconvolution technique,[24] and discrimination between Lorentzian, Gaussian, and Voigtian band profiles. The influence of the spectrometer function on the experimentally

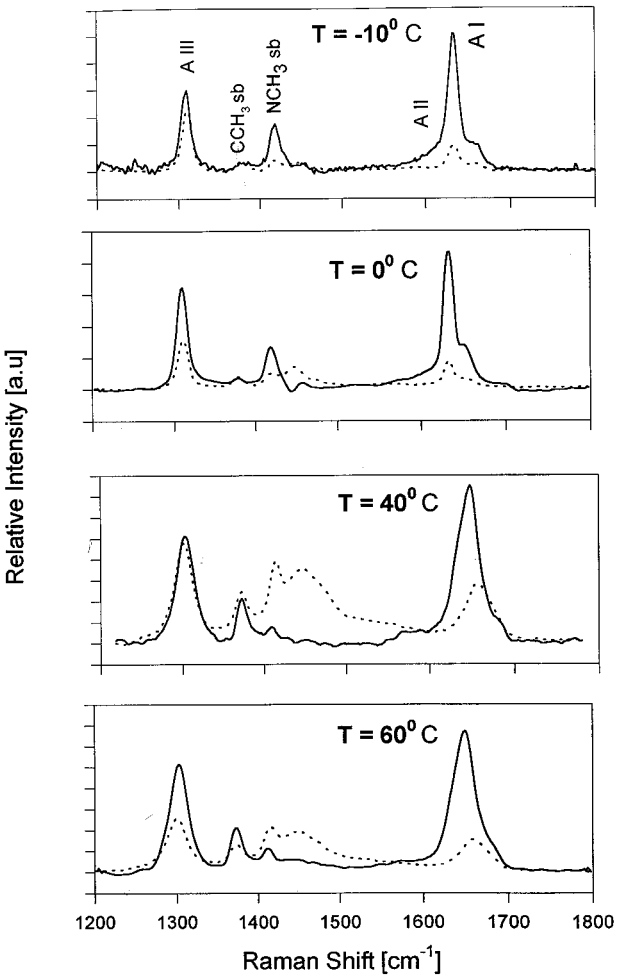

Figure 2. Isotropic (—) and anisotropic (•••) Raman spectra of neat NMA taken with 457 (10, 40, and 60 °C) and 383 nm (−10 °C) excitation at the indicated temperatures. The most prominent bands are labeled as follows: A I, A II, and A III for amide I, II, and III; CCH_3 sb and NCH_3 sb for the Raman bands of the symmetric bending modes of the C- and N-methyl groups, respectively.

observed band shapes could be neglected because the spectral bandwidth was less than one-fourth the half-widths of all Raman and IR bands investigated.[25] The relative intensities of the Raman bands were derived from their areas. The depolarization ratio (DR), ρ, was then calculated as

$$\rho = I_{per}/I_{par} \tag{1}$$

where I_{per} and I_{par} denote the intensities measured with the polarizer oriented perpendicular and parallel to the incident polarization, respectively.

The collection cones of the collimator lenses utilized in the Raman spectrometers have a half-angle of 15°. This allows a rather exact determination of the depolarization ratios.[26] To eliminate possible errors due to an insufficient depolarization by the polarization scrambler, the latter was adjusted so that the measured DR of the 216 cm^{-1} line in the CCl_4 Raman spectrum (for the University of Michigan spectrometer) and of the 655 cm^{-1} Raman line of CS_2 (for the University of Bremen spectrometer) were identical with their expectation values of 0.75 and 0.05, respectively.[27]

Results and Discussion

A. Raman and FT-IR Spectra of Neat NMA and NMA in CD_3CN. Figure 2 compares the isotropic and anisotropic Raman spectra of neat NMA taken at 60, 40, 0, and −10 °C with 457 nm excitation. While the anisotropic spectrum is identical with the depolarized (i.e., I_{per}) spectrum, the intensities of bands in the isotropic spectra were obtained by

$$I_{iso} = I_{par} - (4/3)I_{per} \tag{2}$$

All spectra are dominated by the amide I and amide III bands. At 40 °C, the former is observed at 1645 cm^{-1} while the latter appears around 1300 cm^{-1}. Their frequencies depend on temperature, amide I increasing and amide III decreasing with rising temperatures. These effects are consistent with a weakening of intermolecular hydrogen bonds.

All spectra of the liquid phase (T > 30 °C) look rather similar but differ from those of the solid crystallized phase. This is particularly true of the relative intensities of the bands between 1350 and 1500 cm^{-1}, which all result from CH_3 bending (b) vibrations of the C- and N-methyl groups. In the liquid phase the CCH_3 symmetric bend (sb) at ∼1380 cm^{-1} is significantly more intense than the NCH_3 sb at ∼1420 cm^{-1}. Its DR value is close to 0.33, which indicates that the intensity stems predominantly from Franck−Condon type coupling with the $\pi \rightarrow \pi^*$ transition in the far-UV region.[10i] In contrast, the NCH_3 sb band appears more depolarized. The phase transition reverses both intensities and DR values, so that the CCH_3 sb band appears more depolarized in the solid-state spectra.

Other changes in the spectrum are also noteworthy. Amide I and amide III become narrower upon crystallization, and amide I exhibits a significant change in its band shape. Amide II is rather weak in all Raman spectra and appears solely as a shoulder on the low-frequency side of amide I in the isotropic spectra. A rather broad band centered at 1530 cm^{-1} shows up in the anisotropic spectra of liquid NMA and disappears completely at low temperatures in the spectra of crystallized NMA.

Figure 3 shows the FT-IR spectrum of liquid NMA taken at 30 °C. In contrast to the Raman spectra, amide II is now clearly visible. Its relative intensity is intermediate between that of

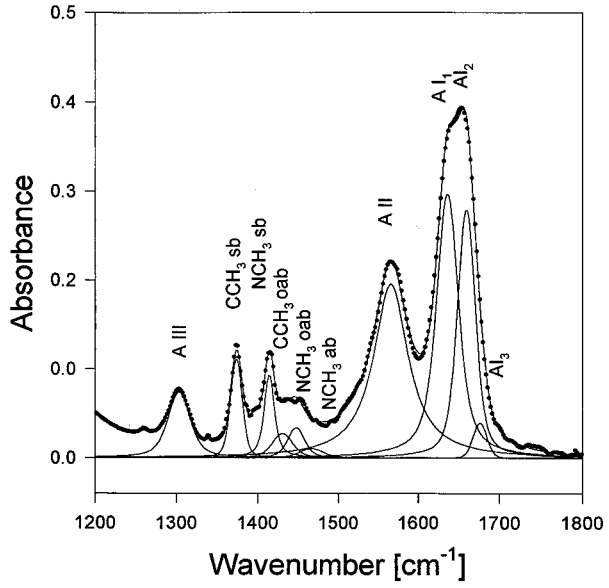

Figure 3. FT-IR spectrum of liquid NMA measured at 30 °C. The data were taken from an earlier study.[10i] The solid line and the single bands displayed therein result from the line shape analysis outlined in the text. The dots are experimental points. The labeling of the prominent bands is the same as used for Figure 2, and assignments are based on ref 10i.

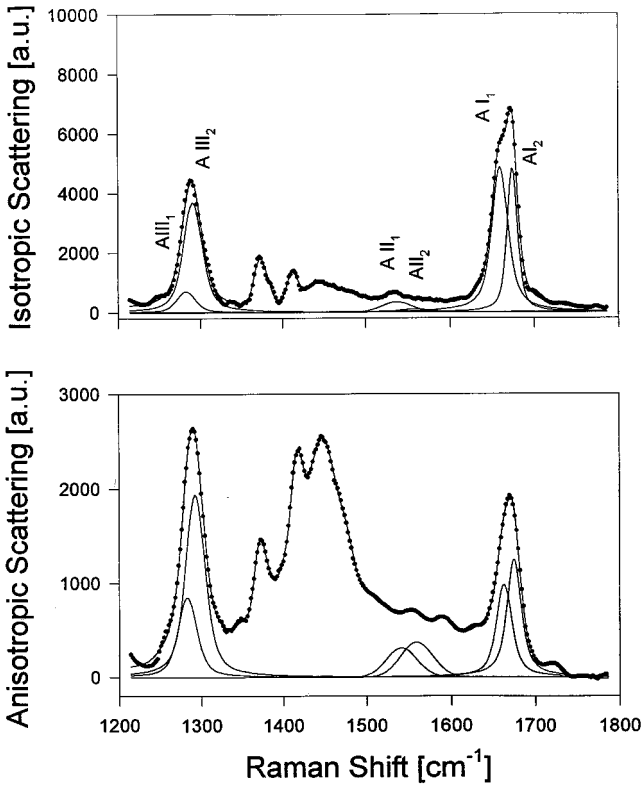

Figure 4. Isotropic and anisotropic Raman spectra of NMA in CD_3CN measured with 457 nm excitation at 30 °C. The solute concentration was 3.0 M. The solid line and the single bands displayed therein result from the line shape analysis outlined in the text. The dots are experimental points.

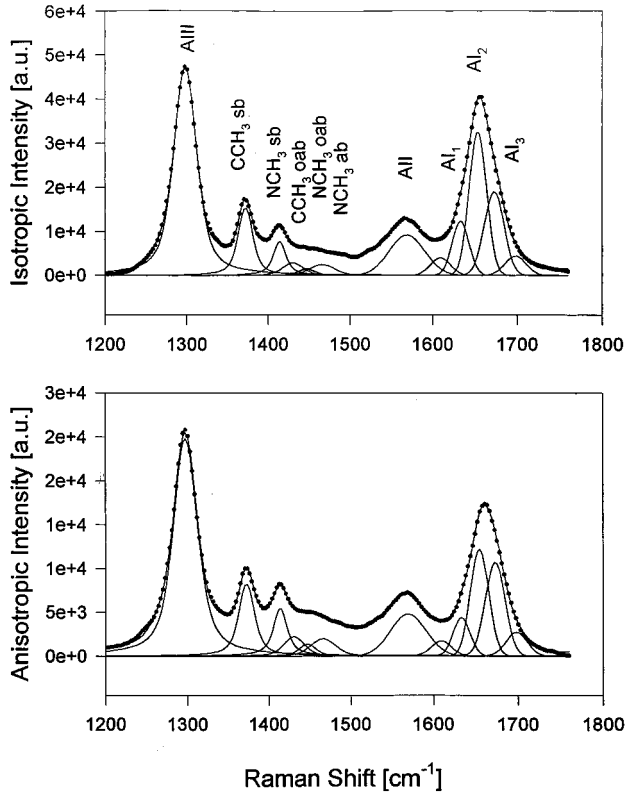

Figure 5. Isotropic and anisotropic UV-Raman spectra of liquid NMA measured with 244 nm excitation. The original data were taken from ref 10i. The solid line and the single bands displayed therein result from the line shape analysis outlined in the text. The dots are experimental points.

amide I and amide III. The methyl bands are clearly discernible and the broad band at 1530 cm^{-1} is evident as a shoulder on amide II. (In this and other spectra, not all component bands are shown.)

Figure 4 displays the isotropic and anisotropic Raman spectra of NMA in 3.0 M CD_3CN. Similar to liquid NMA, amide I is intense while amide II is barely detectable. Moreover, amide I appears as a doublet in the isotropic spectrum.

All Raman data (i.e., spectra measured at 60, 50, 40, 30, 25, 22, 15, 8, 0. and −10 °C) and FT-IR data were subjected to a self-consistent analysis by adopting the following strategy. First, we refitted the Raman spectra of liquid NMA reported in our recent paper,[10i] which were measured with different excitation wavelengths, together with the present spectra measured at 30 °C. Here we used the isotropic rather than the polarized spectra as was done in the above study. As an example, Figure 5 shows the isotropic and anisotropic Raman spectra of liquid NMA measured with 244 nm excitation.[10i] Corresponding Raman bands in the isotropic and anisotropic spectra observed with different excitation wavelengths were fit with identical band shapes and half-widths. Slight deviations in the band position (±3 cm^{-1}) were allowed in order to account for some uncertainties in the frequency calibration of the spectra that were recorded with different spectrometers.

Next, the resulting spectral parameters (i.e., frequencies, half-widths, and band shapes) were then used as a starting point in a fit of the FT-IR data shown in Figure 3. It turned out that appropriate fitting required some changes in the spectral parameters of amide I and amide III, while the remainder of the spectrum could be well reproduced without changing parameters. These discrepancies for amide I and amide III are physically expected and will be discussed in more detail below.

To fit the Raman data measured at different temperatures, we assumed that only the spectral parameters of the amide bands changed with temperature whereas those of the methyl bands and the unknown broad band at 1530 cm^{-1} were constant. This yielded quite successful fits to all spectra. The fits to the isotropic and anisotropic Raman spectra taken at −10 and 30 °C, as well as the underlying spectral bands, are displayed in Figures 6 and 7. Their spectral parameters are given in Table 1. Table 2 lists the depolarization ratios of the amide bands for all temperatures employed.

Finally, we fitted the isotropic and anisotropic spectrum of NMA in CD_3CN with the same band shape model. The spectral parameters are listed in Table 3.

B. Spectral Analysis of Amide I. *Spectral Decomposition: Neat NMA.* The shape of the amide I band is clearly asymmetric. Appropriate fitting requires a number of Gaussian subbands, of which we designate three as amide I modes, Sb_1(I), Sb_2(I), and Sb_3(I). At 30 °C the corresponding frequencies in the isotropic spectrum are 1634 cm^{-1} (Sb_1(I)), 1651 cm^{-1} (Sb_2(I)), and 1674 cm^{-1}(Sb_3(I)). This is also supported by the Fourier self-deconvolution of the amide I band profile (data not shown). (The 1610 cm^{-1} subband may be due to a 992 + 628 = 1620 combination;[10c] it is expected to increase by 18 cm^{-1} in the solid state[10c] and is found to increase by 10 cm^{-1}.) While we found the same positions for Sb_1(I) and Sb_3(I) in the anisotropic spectrum, Sb_2(I) is observed at a higher frequency, viz., 1656 cm^{-1}, and exhibits a somewhat larger half-width. The three subbands are also found in the IR spectrum. The frequencies of Sb_1(I) and Sb_3(I) are identical with the values obtained in the isotropic and anisotropic Raman spectra. Sb_2-(I) is at 1659 cm^{-1}, which is close to this subband's position in the anisotropic Raman spectrum. (We note that a similar

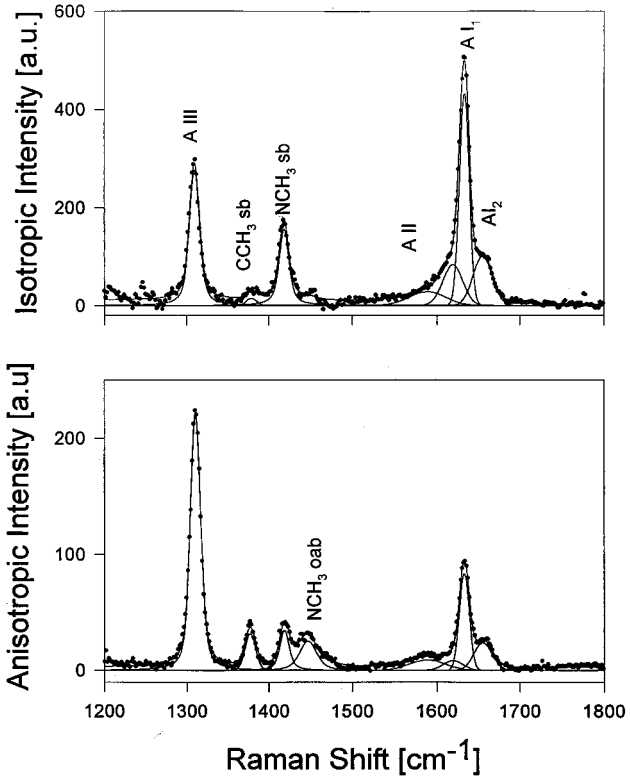

Figure 6. Spectral analysis of the isotropic and anisotropic Raman spectra of crystallized NMA measured with 383 nm excitation at −10 °C. The single bands and the solid lines result from the fitting procedure described in the text. The dots are experimental points.

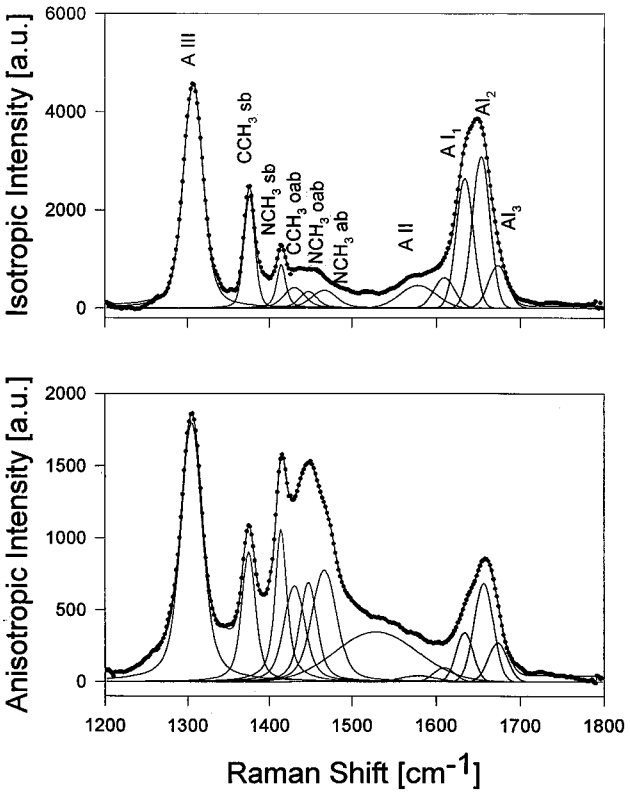

Figure 7. Spectral analysis of the isotropic and anisotropic Raman spectra of liquid NMA measured with 457 nm excitation at 30 °C. The single bands and the solid lines result from the fitting procedure described in the text. The dots are experimental points.

subband structure, though not with the same frequencies, has been detected by two-dimensional correlation spectroscopy[28a,b]).

TABLE 1: Spectral Parameters Obtained from the Fit to the Isotropic and Anisotropic Raman Spectra Taken at −10 and 30 °C[a]

mode[b]	ν_{iso} (cm^{-1})	Γ_{iso}[c] (cm^{-1})	ν_{aniso} (cm^{-1})	Γ_{aniso}[c] (cm^{-1})	ρ
(A) Solid Phase (−10 °C)					
amide I (Sb$_2$)	1656	27.3	1656	27.2	0.17
amide I (Sb$_1$)	1633	13.4	1633	13.4	0.15
amide II	1589	51.0	1589	51.0	0.23
NCH$_3$ ab	1475	26.9	1475	26.9	0.75
NCH$_3$ oab	1447	21.1	1447	21.1	0.66
CCH$_3$ oab	1430	25.6	1430	25.6	0.60
NCH$_3$ sb	1419	11.9	1419	11.9	0.16
CCH$_3$ sb	1377	14.2	1377	14.2	0.56
amide III	1310	12.6	1311	12.5	0.38
(B) Liquid Phase (30 °C)					
amide I (Sb$_3$)	1674	26.9	1674	26.9	0.25
amide I (Sb$_2$)	1651	21.5	1656	25.0	0.18
amide I (Sb$_1$)	1634	23.5	1634	23.5	0.12
amide II	1578	50.1	1578	50.0	0.10
NCH$_3$ ab	1466	31.0	1466	31.0	0.51
NCH$_3$ oab	1447	21.1	1447	21.1	0.47
CCH$_3$ oab	1430	25.6	1430	25.6	0.48
NCH$_3$ sb	1414	10.5	1414	14.4	0.50
CCH$_3$ sb	1374	14.5	1374	17.0	0.31
amide III	1307	25.1	1305	27.0	0.27

[a] From Figures 5 and 6. [b] sb, symmetric bending; ab, in-plane antisymmetric bending, oab: out-of-plane antisymmetric bending. [c] Bandwidth at half-maximum, $\Gamma = ((\Gamma_{Lor})^2 + (\Gamma_{Gau})^2)^{1/2}$ (Lor, Lorentzian; Gau, Gaussian), for the isotropic and anisotropic components, respectively.

TABLE 2: Depolarization Ratios of Amide I and Amide III Bands Observed at Different Temperatures between −10 and 60 °C

T (°C)	Sb$_1$ (I)	Sb$_2$ (I)	Sb$_3$ (I)	amide III
−10	0.15	0.17		0.38
0	0.14	0.16		0.28
8	0.12	0.16	0.24	0.25
15	0.12	0.16	0.22	0.28
22	0.12	0.21	0.29	0.36
25	0.10	0.16	0.16	0.26
30	0.10	0.18	0.25	0.27
40	0.13	0.25	0.36	0.31
50	0.12	0.21	0.26	0.31
60	0.12	0.16	0.31	0.31

TABLE 3: Spectral Parameters Derived from the Fit to the Isotropic and Anisotropic Spectra of 3.0 M NMA in CD$_3$CN[a]

mode[b]	ν_{iso} (cm^{-1})	Γ_{iso}[c] (cm^{-1})	ν_{aniso} (cm^{-1})	Γ_{aniso}[c] (cm^{-1})	ρ
amide I (Sb$_2$)	1675	12.2	1676	16.4	0.22
amide I (Sb$_1$)	1660	20.0	1665	18.5	0.16
NCH$_3$ ab	1474	26.8	1474	26.8	0.66
NCH$_3$ oab	1453	25.5	1453	25.5	0.59
CCH$_3$ oab	1436	30.0	1436	30.0	0.61
NCH$_3$ sb	1412	15.0	1415	15.9	0.53
CCH$_3$ sb	1371	15.7	1371	15.7	0.36
amide III$_2$[d]	1291	23.6	1291	25.0	0.33
amide III$_1$[d]	1282	23.4	1282	23.4	0.37

[a] The amide II parameters are not tabulated because they cannot be determined with suffcient accuracy. [b] sb, symmetric bending; ab, in-plane asymmetric bending; oab, out-of-plane antisymmetric bending. [c] Bandwidth at half-maximum, $\Gamma = ((\Gamma_{Lor})^2 + (\Gamma_{Gau})^2)^{1/2}$ (Lor, Lorentzian; Gau, Gaussian), for the isotropic and anisotropic component, respectively. [d] Amide III also exhibits two subbands due the existence of two different species.

These results are somewhat different from those reported earlier by Chen et al.[10i] In that study the spectral analyses were applied to polarized and depolarized spectra taken at ambient temperature. This yielded two main subbands, a polarized one

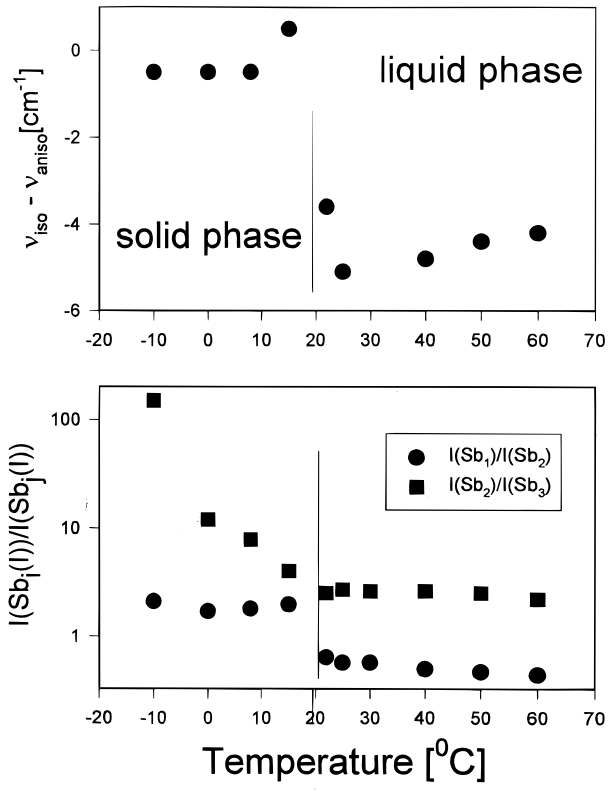

Figure 8. Temperature dependence of $\Delta\nu_{NCE}$ of $Sb_2(I)$ (upper panel) and intensity ratios of the amide I subbands (lower panel). The melting temperature is marked by a vertical line.

at 1646 cm^{-1} and a depolarized one at 1658 cm^{-1}. Apparently these subbands correspond to $Sb_2(I)$ in the isotropic and anisotropic Raman spectra. Chen et al.[10i] also found a subband at 1630 cm^{-1}, which they described as weak in the Raman and strong in the IR spectrum. The present data allow a more appropriate determination of the spectral parameters of this band due to its strong appearance in the Raman spectrum of solid NMA. From this we obtained its frequency as 1634 cm^{-1}, and its contribution to the overall band shape of amide I turns out to be much more significant than that anticipated by Chen et al. The subband $Sb_3(I)$ was not recognized in the earlier study, but despite its relatively low intensity its existence is now apparent, in particular in the Raman spectra taken at higher temperatures.

Chen et al.[10i] interpreted their two major amide I subbands of liquid NMA as resulting from an NCE, i.e., isotropic and anisotropic scattering appearing at different frequencies.[16] This interpretation must still be considered correct, but it applies only to $Sb_2(I)$, which indeed shows a clear difference between its isotropic and anisotropic frequencies. In full accordance with what one expects theoretically,[16b,c] the IR $Sb_2(I)$ band is close to (perhaps slightly higher than) the corresponding band position in the anisotropic Raman spectrum. $Sb_1(I)$ and $Sb_3(I)$, however, show no detectable NCE.

The temperature dependence of the NCE splitting of $Sb_2(I)$, denoted as

$$\Delta\nu_{NCE}(I) = \nu_{iso}(I) - \nu_{aniso}(I) \qquad (3)$$

is shown in Figure 8 (upper panel). Within the limit of accuracy, $\Delta\nu_{NCE}(I)$ exhibits a temperature independent value of -5 cm^{-1} in the liquid phase, but it is reduced in the solid phase because $Sb_2(I)$ shifts from 1651 to 1656 cm^{-1} in the isotropic and hardly shifts in the anisotropic spectrum. The DRs of the subbands are different: $Sb_1(I)$ is the most polarized one with an average ρ value of 0.12, ρ of $Sb_2(I)$ varies between 0.16 and 0.25 with maxima at 20 and 40 °C, and ρ of $Sb_3(I)$ ranges between 0.16 and 0.36, showing a slight increase with temperature in the liquid phase (Table 2). The bandwidths of the subbands are nearly independent of temperature in the liquid phase, but crystallization causes a significant narrowing of $Sb_1(I)$ (Table 1).

The temperature dependence of the intensity ratio $I[Sb_1(I)]/I[Sb_2(I)]$ clearly reflects the solid ⇔ liquid phase transition. As shown in Figure 8 (lower panel), it is quite constant below 15 °C, drops off between 15 and 22 °C, and shows a slight decrease with rising temperature. The melting occurs at somewhat lower temperatures than the expected 28 °C. The ratio $I[Sb_2(I)]/I[Sb_3(I)]$ is constant in the liquid phase. Crystallization causes it to increase significantly. In the solid state, $Sb_3(I)$ disappears at -10 °C. These observations indicate that the subbands result from different NMA species, which we designate as C_j ($j = 1, 2, 3$).

Spectral Decomposition: NMA in Acetonitrile. The asymmetric band shape of amide I can be accounted for by two Voigtian subbands (Figure 4). The subband at lower energies appears at 1660 cm^{-1} in the isotropic and 1665 cm^{-1} in the anisotropic spectrum, thus showing an NCE of -5 cm^{-1}. The second subband, at 1675 cm^{-1}, shows a very small NCE. Both subbands have somewhat smaller half-widths than their counterparts in liquid and aqueous NMA.[10i] The DR values for these bands are 0.16 and 0.22, respectively (cf. Table 3).

Intermolecular Coupling in the Crystalline Phase of NMA. To develop an understanding of the above findings, we start with a spectral analysis of crystalline NMA based on the structure reported by Katz and Post[11a] (Figure 1). They found that below 10 °C crystalline NMA shows a regular chain structure incorporating CO···HN hydrogen bonds between NMA molecules. Two of these hydrogen-bonded chains are in pairs antiparallel to each other, separated by $c/2 + b/2$. With four molecules per unit cell and an inversion center, the normal modes can be classified in terms of irreducible representations of the D_{2h} point group, viz., A_g, B_{1g}, B_{2g}, B_{3g}, A_u, B_{1u}, B_{2u}, and B_{3u}.[29] Since the unit cell has a center of inversion, the mutual exclusion rule applies. Of the in-plane modes, two are IR active: B_{3u}, in which the phase relationships between all four amide groups (*A*, *B*, *C*, and *D* in Figure 1) result in transition dipole moments that are additive along the *a*-axis (designated ↑↑↑↑), and B_{1u}, in which the phases are ↑↓↓↑ and the transition moments are additive along the *c*-axis. Since the amide I transition moment makes an angle of ∼20° with the C═O bond,[10b] it is clear that the intensity of the B_{1u} mode will be close to zero. The in-plane Raman-active modes are of A_g (↑↑↓↓) and B_{2g} (↑↓↑↓) symmetry, with the former generally expected to be the stronger.

The nature of the intermolecular coupling provides insights into the assignments of these modes. The most important interaction is transition dipole coupling (TDC),[1a] which has been shown to dominate amide I splittings in polypeptides.[1b] However, in distinction to previous analyses,[10b] the original polypeptide interaction formalism is not applicable here because of the different geometrical arrangements of the peptide groups. If we consider the closest TDC interactions (the result is not qualitatively different if farther interactions are included), these are between molecules such as *C* and *D* (with each NMA experiencing two interactions at a separation of 4.805 Å) and molecules such as *C* and *A* (with four interactions at a separation of ∼5.0 Å). Taking into account the geometric factor in the TDC interaction,[1a] the potential energy of the *C*−*D* interaction

is always negative for B_{3u} and A_g modes while the $C-A$ interaction is positive for B_{3u} and negative for A_g. Thus, we expect the B_{3u} mode to have a higher frequency than the A_g mode. Polarized IR studies on single crystals[10b] clearly place the B_{3u} mode at 1645−1650 cm^{-1} (at −100 °C), with the B_{1u} mode (barely visible) at 1632 cm^{-1}, and it is therefore compelling to assign the strong 1633 cm^{-1} Raman band to the A_g mode. We note that this is the reverse of the polypeptide case,[1b] in which the "in-phase" amide I mode of β-sheet polypeptides has the lowest frequency.

The assignment of $Sb_1(I)$ (1633 cm^{-1} at −10 °C) to the A_g mode is supported by its DR for the following reason. The Raman tensor of an A_g mode in D_{2h} symmetry is[30]

$$\alpha = \begin{pmatrix} \alpha_{xx} & 0 & 0 \\ 0 & 0 & 0 \\ 0 & 0 & \alpha_{zz} \end{pmatrix} \quad (4)$$

where we assume that, since amide I modes are confined to the xz plane, $\alpha_{yy} = 0$. If α_{xx} and α_{zz} have the same sign, one expects $\rho = 0.125$ for $\alpha_{xx} = \alpha_{zz}$ and $\rho = 0.33$ for α_{xx} or $\alpha_{zz} = 0$. Hence the experimental DR values of 0.10−0.13 suggest that $\alpha_{xx} \approx \alpha_{zz}$.[31]

The situation is less clear for $Sb_2(I)$. With our choice of the coordinate system the Raman tensor of the B_{2g} mode would be

$$\alpha = \begin{pmatrix} 0 & 0 & \alpha_{xz} \\ 0 & 0 & 0 \\ \alpha_{zx} & 0 & 0 \end{pmatrix} \quad (5)$$

Thus its DR has to be 0.75. This is apparently not the case. This could result if the symmetry of the unit cell is somewhat relaxed from strict D_{2h}. Two lines of evidence support this possibility. First, a recent study[11b] has shown that static disorder is present in the crystal, with a ∼10% occupancy of the alternative orientation at both −63 and −163 °C. Second, and perhaps more important, it was noted in the original structure determination[11a] that a short methyl−methyl contact implied an "interleaving of hydrogen atoms of the two methyl groups, such as would result from a 60° rotation of one group relative to the other". Since normal mode calculations[10i,32] show that the amide I eigenvector contains contributions from CCH b and NCH b coordinates that are of the same magnitude as those from CO stretch (s) and CN s, it is not surprising that the amide I modes would reflect a lower symmetry than D_{2h} due to the rotations of the methyl groups. As we will show below, our Raman data provide evidence that such torsional distortions of the methyl groups indeed occur.

The above symmetry lowering would cause all amide I species (i.e., A_g, B_{2g}, B_{1u}, B_{3u}) to mix into one common representation. The corresponding Raman tensor would then be

$$\alpha = \begin{pmatrix} \alpha_{xx} & 0 & \alpha_{xz} \\ 0 & 0 & 0 \\ \alpha_{zx} & 0 & \alpha_{zz} \end{pmatrix} \quad (6)$$

The low DR value of $Sb_2(I)$ now suggests that contributions from off-diagonal elements in eq 6 are negligible so that the intensity of this subband stems predominately from the diagonal elements. Thus, the presence of $Sb_2(I)$ reflects the lower symmetry since this mode would not be detectable in the case of a pure D_{2h} symmetry (because α_{xx} and α_{zz} would be zero, and α_{xz} and α_{zx} would be negligible or else we would have to observe a DR of 0.75).

Finally, we note that the crystal undergoes a phase transition at ∼10 °C.[11a] Although this results in a less ordered structure, with a slightly longer hydrogen bond (by ∼0.05 Å),[11a] we see no change in the Raman spectrum at this point, the major change occurring at the transition to the liquid.

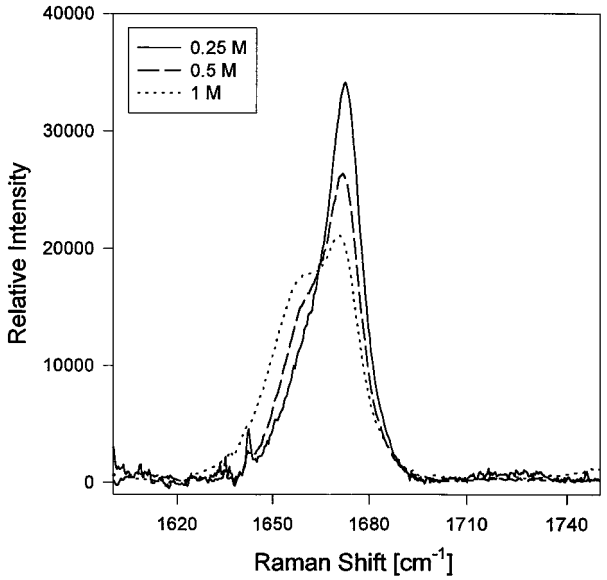

Figure 9. Amide I band profile of NMA in CH_3CN measured at the indicated concentrations with 488 nm CW excitation at room temperature.

Intermolecular Coupling in Acetonitrile Solution. Before discussing the situation in neat NMA, it is useful to consider the spectrum of NMA in CD_3CN. As noted above, there are two subbands in the observed amide I band of a 3.0 M solution.

Two arguments support the assignment of the higher frequency component at 1675 cm^{-1} to a monomeric NMA species. First, UV-resonance Raman spectra measured in very dilute solution (10 mM), which makes oligomerization unlikely to occur, indicate only a single band at 1672 cm^{-1}.[10e] This is in agreement with our dilution experiments shown in Figure 9, which overlays the amide I band profiles of NMA in CH_3CN measured at 0.25, 0.50, and 1.0 M concentrations (deuteration of the methyl group is not necessary for this experiment). This clearly shows that the relative intensity of $Sb_3(I)$ increases with lower concentrations, indicating that it results from the species predominant in dilute solution. Second, the frequency of this band is just what is expected for a solvent-induced shift from the gas-phase frequency of 1722 cm^{-1}.[33] We have performed HF/6-31+G* reaction field calculations on NMA in spherical cavities of different radii (a_0) in solvent environments of varying dielectric constant (ϵ). For $\epsilon = 36$ (that of CH_3CN), the ratio ν(free)/ν(solvent) is 1.0340 for $a_0 = 3.12$ Å (based on the dimensions of the NMA molecule) and 1.0185 for $a_0 = 3.62$ Å (based on the molar density and mass, which probably overestimate the cavity size for a relatively freely rotating NMA molecule). The observed ratio of 1722/1672 = 1.0299 is compelling evidence for assigning the 1675 cm^{-1} band to monomeric NMA.

The lower frequency component, which shows an NCE of −5 cm^{-1}, surely arises from a hydrogen-bonded species, at least a dimer. Comparison of the frequency shift on hydrogen bonding for $\epsilon = 1$[10f] with that in a medium of high ϵ[32] shows that in the latter it is smaller than in the former and well within the range observed, viz., 1675/1662.5 = 1.0075. The question is what gives rise to the NCE.

As shown by McHale,[16b] the influence of intermolecular vibrational coupling on the frequencies of isotropic and aniso-

tropic scattering as well as on IR absorption can be described by

$$\nu_{iso} = \nu_0 + \frac{N}{2m\nu_0}\langle V_{12}\rangle$$

$$\nu_{aniso} = \nu_0 + \frac{N}{2m\nu_0}\langle V_{12}P_2(\cos\Theta_{12})\rangle$$

$$\nu_{IR} = \nu_0 + \frac{N}{2m\nu_0}\langle V_{12}P_1(\cos\Theta_{12})\rangle \qquad (7)$$

where ν_0 is the frequency of the unperturbed isolated vibration, N is the number of molecules, m is the effective mass for the mode, and $P_n(\cos\Theta_{12})$ ($n = 1, 2$) are Legendre polynomials with respect to the angle between the respective transition dipole moments. The interaction potential V_{12} is determined by transition dipole coupling[1a]

$$V_{12} = \gamma^2\frac{\hat{e}_1\hat{e}_2 - 3(\hat{e}_1\cdot\hat{n}_{12})(\hat{e}_2\cdot\hat{n}_{12})}{R_{12}^3} \qquad (8)$$

where γ denotes the transition dipole moment $\delta\mu/\delta Q$ (Q is the vibrational coordinate) of the two vibrational oscillators, $\hat{e}_1$ and $\hat{e}_2$ are the corresponding unit vectors, n_{12} is the unit vector along the line connecting the two oscillators, and R_{12} is the distance between them.

The interaction potential V_{12} may be either negative or positive depending on the arrangement of the transition moments determined by the local order in the liquid. Model calculations by Torii and Tasumi[34] indicated that for the carbonyl vibration of liquid acetone negative intermolecular coupling (and thus negative $\Delta\nu_{NCE}$) results from local molecular order imposed by energetically favorable interactions between permanent dipoles. In contrast, the CO s Raman band of liquid methanol exhibits a positive NCE ($\Delta\nu_{NCE} > 0$) because hydrogen bonding in this system imposes a dominating positive contribution to $\langle V_{12}\rangle$.

We assume, therefore, that the negative NCE of the 1660/1665 cm^{-1} band arises from a favorable arrangement of neighboring NMA molecules. The most likely structure to produce this is a hydrogen-bonded dimer, since such an arrangement, whether with peptide groups coplanar as in the crystal or perpendicular to one another as proposed for an isolated dimer,[35] is also a favorable dipolar structure and will lead to a negative $\langle V_{12}\rangle$. Of course, if such dimers (or possible short oligomers) interact laterally, they will undoubtedly do so in an average antiparallel arrangement, which will also contribute to a negative $\langle V_{12}\rangle$. Since the non-hydrogen-bonded CO of the dimer has a frequency essentially the same as that of the monomer,[36] overlap with the monomer band may account for its small NCE.

Intermolecular Coupling in Liquid NMA. The above analyses of the spectra of crystalline NMA and of its acetonitrile solutions provide a basis for identifying the molecular species, C_1, C_2, and C_3, associated with the three amide I band components in liquid NMA.

The C_3 species, represented by the 1674 cm^{-1} subband, is to be associated with the presence of monomers. This follows from our discussion of the same band in CD_3CN solutions of NMA. Its intensity is due to the monomer content plus the non-hydrogen-bonded CO end groups of oligomers. The absence of an NCE indicates that the monomers are not ordered with respect to each other.

The C_2 species, represented by the 1651/1656 cm^{-1} subband, is clearly associated with a hydrogen-bonded structure. Its lower frequency than the 1660/1665 cm^{-1} band of the CD_3CN solution could be due to a difference in dimer structure (for example, the perpendicular orientation of peptide planes in the isolated dimer[35] vs a parallel orientation as in the crystal[11a]) or to the preponderance of higher oligomers. Or, it could be associated with the likely lateral antiparallel arrangement of oligomers, which will also contribute to a negative $\langle V_{12}\rangle$. Logan[16c] has shown that in this situation the IR band appears at a slightly higher frequency than the anisotropic band, which is what we observe experimentally.

The C_1 species, represented by the 1634 cm^{-1} subband, is most likely associated with long oligomeric hydrogen-bonded chains. Its lack of an NCE may be due to a tendency for such longer chains to have parallel as well as antiparallel neighbors, thus giving rise to positive as well as negative $\langle V_{12}\rangle$.

Depolarization Ratios. All amide I bands appear polarized, but the DR values of the subbands increase with increasing frequency (cf. Table 1). At 30 °C we found $\rho(Sb_1) = 0.12$, $\rho(Sb_2) = 0.18$. and $\rho(Sb_3) = 0.25$. As outlined by Chen et al.,[10i,31] DR measurements far from resonance may aid in identifying contributions from electronic transitions at much higher energies. DR values between 0.125 and 0.33 indicate that at least two electronic transitions are involved (we neglect the possibility of degenerate transitions in this context). Possible candidates for amide I are the $\pi \rightarrow \pi^*$ transition (190 nm) and a more localized transition at even higher energies which mainly involves the CO bond.[10i] In this case one expects the DRs to approach 0.33 upon excitation in the UV region. Indeed the corresponding DRs of the liquid NMA spectra taken with 244 nm excitation (Figure 4) were found to be 0.25 (Sb_1), 0.30 (Sb_2), and 0.35 (Sb_3), thus reflecting the now predominant contribution of the $\pi \rightarrow \pi^*$ transition.[10i]

It is noteworthy that the above DR values are not much different from corresponding values obtained for NMA in aqueous solution.[10i] This is surprising because amide I of neat NMA appears much more intense. This enhancement therefore comes in approximately equal parts from both electronic transitions to which the amide I mode is vibronically coupled. This notion is consistent with the Raman data on NMA in CD_3CN. The relative intensity of amide I in these spectra is even larger than observed for liquid NMA, whereas corresponding DR values are similar.

C. Analysis of Amide II and III. Although it appears only weakly in the Raman spectrum of the crystal, the amide II mode can be well characterized from the polarized IR spectrum.[10b] The B_{1u} mode is found at 1584 cm^{-1} (at −100 °C) and, as expected from the TDC interactions for this mode, is at a higher frequency than the B_{3u} mode at 1573 cm^{-1}. The exact value of the latter frequency is complicated by the presence of a B_{3u} band at 1521 cm^{-1}, which probably arises from a Fermi resonance of the combination of the strong 787 cm^{-1} B_{3u} IR and the B_{2g} Raman amide V fundamentals with the B_{3u} amide II fundamental, thus displacing the latter to a higher (i.e., 1573 cm^{-1}) frequency. The 1589 cm^{-1} band in the Raman spectrum is undoubtedly the A_g mode, and its similar frequency to that of the B_{1u} mode mirrors the situation with the amide I mode.

Amide II also appears only weakly in the visible Raman spectrum of neat NMA. The spectral parameters were obtained from the fit to the isotropic and anisotropic spectra taken with 244 nm excitation (Figure 5) and used in the fit to the visible spectra of liquid NMA. The fit comprises a single broad Gaussian band at 1578 cm^{-1} of 50 cm^{-1} half-width, which

shows no detectable NCE. A similar result is obtained from the fit to the IR spectrum (Figure 3), although its different frequency (1566 cm^{-1}) may be indicative of the oligomeric heterogeneity in the sample. The data do not allow decomposition into subbands even though the large half-widths may also indicate such conformational heterogeneity. The spectra of NMA in CD_3CN do not allow an unambiguous identification of amide II.

The amide III mode leads to an intense band at 1307 cm^{-1} in the Raman spectrum of neat NMA but a weak one in the IR spectrum. The band can be nicely fitted by a single component showing that it is less sensitive to oligomeric composition than amide I. In the liquid phase it shows a small but clearly discernible positive NCE of $\Delta\nu_{NCE} = 2-3$ cm^{-1}. Its isotropic and anisotropic frequencies decrease from 1307 and 1305 cm^{-1} at 30 °C to 1302 and 1300 cm^{-1} at 60 °C. Crystallization causes a frequency upshift to 1310 cm^{-1}, with a small splitting of ~1 cm^{-1}. This may reflect the existence of two subbands associated with different symmetry species.

Amide III is polarized with DR values between 0.28 and 0.35 in the liquid and solid states. This parallels observations for aqueous NMA[10i] and indicates that its intensity is nearly entirely provided by the $\pi \rightarrow \pi^*$ transition in the far-UV.

It is somewhat difficult to classify the NCE effect of amide III for the liquid phase because all the species obtained from the decomposition of amide I contribute to the overall band shape. By comparison with the amide I observation, the overall positive NCE of the liquid phase is most likely to result from some intermolecular coupling associated with C_2. The NMA dimer calculated by Dixon et al.[35] cannot explain our data since it would have its amide III transition dipoles in perpendicular orientation with respect to each other, so that their coupling would be negligible. Thus, we again invoke the model already utilized to explain the NCE of amide I, namely, a local order of dimers or oligomers that is determined by dipole−dipole interactions. If this mimics the lateral arrangement in the crystal, then the amide I permanent dipoles of adjacent (i.e., *c*-axis-related) NMA molecules will be in an energetically favorable orientation. This will result in a TDC interaction for amide I that gives a negative NCE,[34] as observed. However, the amide III transition moment is roughly perpendicular to that of amide I, and we can therefore expect its TDC interaction to yield a positive NCE, as observed. Since the magnitude of its transition moment is much smaller than that of amide I, it is not surprising that $|\Delta\nu_{NCE}(III)| < |\Delta\nu_{NCE}(I)|$.

D. Analysis of the Methyl Bands. The bands in the 1350−1500 cm^{-1} spectral region are assigned to the bending modes of the methyl groups (CCH_3 and NCH_3).[32] In the Raman spectra, we found that crystallization reverses the intensity of the two bands that arise from the methyl symmetric bending modes (Figures 6 and 7). In the liquid phase, the CCH_3 sb at 1374 cm^{-1} is more intense and is known to become resonance enhanced when approaching the UV region.[10h,i] This is reflected by its DR value, which does not deviate much from 0.33. The weaker NCH_3 sb band at 1414 cm^{-1} is significantly more depolarized. Crystallization significantly reduces the intensity of CCH_3 sb and reverses the depolarization ratios of these bands (Table 1).

These changes in relative intensities may be related to the arrangement of the molecules in the crystal structure. As we noted earlier, Katz and Post[11a] suggested that in the crystal some methyl rotation is expected due to the short contact between C- and N-methyl groups of corresponding chains in adjacent unit cells. To investigate the effect of a rotated methyl group on the Raman and IR intensities of the methyl symmetric bending modes, we carried out HF/6-31+G* ab initio calculations of an $NMA(H_2O)_2$ system in which the methyl groups were rotated from equilibrium as follows: (i) 30° rotation of the CCH_3 group, (ii) 30° rotation of the NCH_3 group, (iii) 30° rotation of both methyl groups such that there is a 0° rotation with respect to each other, and (iv) 30° opposite rotations of each methyl group such that there is a 60° rotation with respect to each other.

The ab initio Raman intensities show that the relative intensity of the two bands corresponding to the methyl symmetric bends, $I_r = I(NCH_3\ sb)/I(CCH_3\ sb)$, is equal to 1 for the equilibrium geometry and changes to ~3 when the methyl groups are rotated away from the equilibrium position. Calculations of resonance Raman intensities also show a change in the same direction but of different magnitude. These results would indeed support the idea that the changes in relative intensities of these bands are a result of rotations of the methyl groups in the crystal structure, which would agree with the conclusion of Katz and Post.

The calculated IR intensities, based on the ab initio dipole derivatives and the eigenvectors obtained using a scaled force field, show that when the methyl groups are rotated away from the equilibrium position, the intensity of the band corresponding to NCH_3 sb increases with respect to that of the CCH_3 sb, but never to the point where I_r is >1 ($I_r = 0.24$ for the equilibrium geometry, 0.41 for the C-methyl rotation, 0.30 for N-methyl rotation, and 0.46 for a rotation of both methyl groups). Both bands have nearly equal intensity in the IR spectra of the liquid phase (Figure 3) and also exhibit the same intensity reversal in the IR spectra of the solid NMA.[10a,b]

Thus, while methyl group rotations give rise to changes in I_r in the right direction, the present calculations do not account quantitatively for the changes observed. However, we must keep in mind that these calculations were done on an effectively isolated molecule. In the crystal two other important additional effects may be present: the contact between methyl groups may distort their geometry, and the nonbonded interactions may change the force field experienced by these groups (and therefore the eigenvectors). At this stage it seems reasonable to conclude that we have a qualitative understanding of the underlying origin of the observed intensity changes. Moreover, we note that these methyl group rotations in effect lower the D_{2h} symmetry of the unit cell, thus supporting our conclusions with respect to the presence and depolarization ratio of the $Sb_2(I)$ component of amide I.

The broad band in the Raman spectra of neat NMA comprises three bands at 1430, 1447, and 1466 cm^{-1}. They are assigned to CCH_3 out-of-plane antisymmetric bend (oab), NCH_3 oab, and NCH_3 in-plane symmetric bend, respectively.[32] They appear nearly depolarized in the spectra of the solid phase ($\rho = 0.75$) but show some isotropic scattering in the liquid phase.

Conclusions

The nature of liquid-state structure continues to be a significant and challenging problem, especially in hydrogen-bonded systems. While diffraction techniques can provide important information based on pair distribution functions,[37] vibrational spectroscopy permits a detailed study of molecular organization in both neat and solution states through analysis of the effects of intermolecular interactions on intramolecular vibrational modes.

We have used IR and Raman spectroscopies to study molecular organization in neat NMA, basing our analysis on an understanding of intermolecular coupling in the crystalline

state and in solution in acetonitrile. This was possible by the examination of spectra at different temperatures, by a self-consistent decomposition of bands in the IR and in the isotropic and anisotropic Raman spectra into their underlying components, with determination of their depolarization ratios, and by analysis of noncoincidence effects ($\Delta\nu_{NCE}$) for some of these bands.

The analysis of the spectra of crystalline NMA shows that observed splittings in amide I modes can be understood on the basis of transition dipole coupling between molecules, an interaction mechanism already shown to be important in polypeptides.[1] We assign the strong 1633 cm^{-1} Raman band to the A_g mode and the weak 1656 cm^{-1} band to the B_{2g} mode; the B_{3u} mode is found in the IR[10b] at 1645−1650 cm^{-1}. This analysis provides the basis for treating intermolecular interactions in the liquid phase. The results of depolarization ratio measurements also support a proposed departure from the strict D_{2h} symmetry of the heavy atom structure,[11a] which is confirmed by our ab initio calculations on an NMA molecule with torsionally distorted methyl groups.

The analysis of the spectra of NMA in solution in acetronitrile leads to a clear assignment of the monomer band at 1675 cm^{-1}, both on the basis of dilution experiments as well as on the basis of a comparison of reaction field calculations with the gas-phase frequency. The lower frequency band at 1660 (isotropic), 1665 (anisotropic) cm^{-1}, which increases in intensity with decreasing concentration, is clearly due to a hydrogen-bonded species, most probably a dimer. Its $\Delta\nu_{NCE} = -5$ cm^{-1} is consistent with the head-to-tail arrangement of molecules in the hydrogen-bonded crystal.

These results lead to convincing assignments of the three amide I subbands of neat NMA. The weak 1674 cm^{-1} band is easily associated with the monomer. The 1651/1656 cm^{-1} pair ($\Delta\nu_{NCE} = -4$ cm^{-1}) can be assigned to short oligomeric species, the negative noncoincidence effect indicating well-defined orientational arrangements between neighboring molecules. The third subband, at 1634 cm^{-1} with $\Delta\nu_{NCE} = 0$, is most likely associated with long oligomeric species having parallel as well as antiparallel neighboring hydrogen-bonded chains.

These studies thus provide an independent route for helping to elucidate the local molecular organization in liquid NMA.

Acknowledgment. This research was supported by NSF Grants MCB 9601006 and DMR 967786. Part of this work was carried out when R.S.S. was a Max Kade Fellow at the University of Michigan. The research at the University of Bremen was supported by a grant from the Deutsche Forschungsgemeinschaft (Schw 398/15-1).

References and Notes

(1) (a) Cheam, T. C.; Krimm, S. *J. Chem. Phys.* **1985**, *82*, 1631. (b) Krimm, S.; Bandekar, J. *Adv. Protein Chem.* **1986**, *38*, 181.

(2) Song, S.; Asher, S. A. *J. Am. Chem. Soc.* **1989**, *111*, 4295.

(3) (a) Hildebrandt, P.; Tsuboi, M.; Spiro, T. G. *J. Phys. Chem.* **1990**, *94*, 2274. (b) Mortensen, A.; Faurskov Nielsen, O.; Yarwood, J; Shelley, V. *J. Phys. Chem.* **1994**, *98*, 5221. (c) Mortensen, A., Faurskov Nielsen, O, Yarwood, J; Shelley, J. *J. Raman Spectrosc.* **1995**, *26*, 669.

(4) Wallen, S. L.; Nikiel, L; Lee, Y.-T.; Jonas, J. *J. Raman Spectrosc.* **1995**, *26*, 1019.

(5) (a) Thomas, H. D.; Jonas, J. *J. Chem. Phys.* **1989**, *90*, 4144. (b) Triggs, N. E.; Valentini, J. J. *J. Phys. Chem.* **1992**, *96*, 6922.

(6) Triggs, N. E.; Bonn, N. E.; Valentini, J. J. *J. Phys. Chem.* **1993**, *97*, 5535.

(7) Wang, Y.; Purrello, R.; Geogius, S.; Spiro, T. G. *J. Am. Chem. Soc*. **1991**, *113*, 6368.

(8) Mortensen, A.; Faurskov Nielsen, O.; Yarwood, J.; Shelley, V. *Vib. Spectrosc*. **1994**, *8*, 37.

(9) Ladell, J.; Post, B. *Acta Crystallogr*. **1954**, *7*, 559.

(10) (a) Miyazawa, T.; Shimanouchi, T.; Mizushima, S.-I. *J. Chem. Phys.* **1956**, *24*, 408. (b) Bradbury, E. M.; Elliott, A. *Spectrochim. Acta*. **1963**, *19*, 995. (c) Schneider, B.; Horeni, A.; Pivcova, H.; Honzl, J. *Collect. Czech. Chem. Commun.* **1965**, *30*, 2196. (d) Dudik, J. M., Johnson, C. R.; Asher, S. A. *J. Phys. Chem.* **1985**, *89*, 3805. (e) Mayne, L. C.; Ziegler, L. D.; Hudson, B. *J. Phys. Chem*. **1985**, *89*, 3395. (f) Mirkin, N. G; Krimm, S. *J. Am. Chem. Soc*. **1991**, *113*, 9742. (g) Song, S; Asher, S. A.; Krimm, S.; Shaw, K. D. *J. Am. Chem. Soc.* **1991**, *113*, 1155. (h) Chen, X. G.; Asher, S. A.; Schweitzer-Stenner, R.; Mirkin, N. G.; Krimm, S. *J. Am. Chem. Soc.* **1995**, *117*, 2884. (i) Chen, X. G.; Schweitzer-Stenner, R.; Asher, S. A.; Mirkin, N. G.; Krimm, S. *J. Phys. Chem.* **1995**, *99*, 3074. (j) Jordan, T.; Spiro, T. G. *J. Raman Spectrosc.* **1995**, *26*, 867. (k) Markham, L. M.; Hudson, B. S. *J. Phys. Chem.* **1996**, *100*, 2731. (l) Miyazawa, T. *J. Chem. Phys*. **1960**, *32*, 1647.

(11) (a) Katz, J. L.; Post, B. *Acta Crystallogr*. **1960**, *13*, 624. (b) Hamzaoui, F.; Baert, F. *Acta Crystallogr*. **1994**, *C50*, 757.

(12) Faurskov Nielsen, O; Christensen, D. H.; Rasmussen, O. H. *J. Mol. Struct.* **1991**, *242*, 273.

(13) Ataka, S.; Takeuchi, H.; Tasumi, M. *J. Mol. Struct.* **1984**, *113*, 147.

(14) Häseler, S.; Poglitsch, A.; Bechtold, G.; Peticolas, W. L. *J. Chem. Phys.* **1986**, *84*, 1046.

(15) Harada, I.; Sugawara, Y.; Matsuura, H.; Shimanouchi, T. *J. Raman Spectrosc.* **1975**, *4*, 91.

(16) (a) Wang, C. H.; McHale, J. L. *J. Chem. Phys.* **1980**, *72*, 4039. (b) McHale, J. L. *J. Chem. Phys.* **1981**, *75*, 30. (c) Logan, D. C. *Chem. Phys.* **1989**, *131*, 199.

(17) (a) Sokolowska, A.; Kecki, Z. *J. Raman Spectrosc.* **1993**, *24*, 331. (b) Kecki, Z.; Sokolowska, A. *J. Raman Spectrosc.* **1994**, *25*, 723.

(18) Mirone, P.; Fini, G. *J. Chem. Phys.* **1979**, *71*, 2441.

(19) Fini, G.; Mirone, P. *Spectrochim. Acta A* **1976**, *32*, 625.

(20) Jones, D. R., Wang, C. H.; Christensen, D. H.; Nielsen, O. F. *J. Chem. Phys.* **1976**, *64*, 4475.

(21) Perchard, C; Perchard, J. P. *J. Raman Spectrosc.* **1975**, *6*, 74.

(22) Jentzen, W.; Unger, E.; Karvounis, G.; Dreybrodt, W.; Shelnutt, J. A.; Schweitzer-Stenner, R. *J. Phys. Chem.* **1996**, *100*, 14184.

(23) Unger, E.; et al. Manuscript in preparation.

(24) Kauppinen, J. K.; Moffat, D. J.; Mantsch, H. H.; Cameron, D. G. *Appl. Spectrosc.* **1981**, *35*, 271.

(25) Jentzen, W. Doctoral Thesis, Bremen, 1994.

(26) Dreybrodt, W.; Stichternath, A. *Proceedings of the XIV International Conference on Raman Spectroscopy, Hong Kong*; Yu, N. T., Li, X.-Y., Eds.; Wiley & Sons; New York, 1994; p 1066.

(27) (a) Fukushi, K.; Kimura, M. J. *J. Raman Spectrosc.* **1979**, *8*, 125. (b) Skinner, J. G.; Nilson, W. G. *J. Opt. Soc. Am.* **1968**, *58*, 113.

(28) (a) Noda, I.; Liu, Y.; Ozaki, Y. *J. Phys. Chem*. **1996**, *100*, 8665. (b) Noda, I.; Liu, Y.; Ozaki, Y. *J. Phys. Chem*. **1996**, *100*, 8674.

(29) Wilson, E. B.; Decius, J. C.; Cross, P. C. *Molecular Vibrations*; Dover Publication: New York, 1980.

(30) McClain, W. M. *J. Chem. Phys.* **1971**, *55*, 2789.

(31) Chen, X. G.; Li, P.; Holtz, J. S. W.; Chi, Z.; Pajcini, V; Asher, S. A. *J. Am. Chem. Soc.* **1996**, *118*, 9716.

(32) Mirkin, N. G.; Krimm, S. *J. Mol. Struct.* **1996**, *377*, 219.

(33) Jones, R. L. *J. Mol. Spectrosc*. **1963**, *11*, 411.

(34) (a) Torii, H.; Tasumi, M. *J. Chem Phys.* **1993**, *99*, 8459. (b) Torii, H. *J. Mol. Struct.*: *THEOCHEM* **1994**, *311*, 199.

(35) Dixon, D. A.; Dobbs, K. D.; Valentini, J. J. *J. Phys. Chem.* **1994**, *98*, 13435.

(36) Cheam, T. C.; Krimm, S. J. *Mol. Struct.*: *THEOCHEM* **1989**, *188*, 15.

(37) Bellisent-Funel, M.-C.; Nasr, S.; Bosio, L. *J. Chem. Phys.* **1997**, *106*, 7913.